# Design of Large Ground-Based Space-Frame Radomes

Reuven Shavit

Department of Electrical and Computer Engineering
Ben-Gurion University of the Negev, Beer-Sheva 84105, Israel
(email: rshavit@ee.bgu.ac.il)

***Abstract*- Large radar antennas are generally covered with radomes to protect them from extreme weather conditions and to enable their continuous precision operation without sacrificing their performance. The radomes are assembled from many panels connected together with metallic or dielectric beams because of their large size. The panels are made of thin membranes or type A sandwiches which are optimized for minimum transmission loss over the operational frequency band of the radome. The beams introduce scattering effects that degrade the overall electromagnetic performance of the antenna enclosed in the radome. This paper addresses the problem of the systematical design of the geometry of the beams for minimum scattering and presents the effect of the radome on the radiation pattern of an antenna which is enclosed within.**

***Index Terms* – metal space-frame radome, dielectric space frame radome, tuned sandwich radome, scattering.**

## I. INTRODUCTION

The radomes are assembled from many panels connected together with metal or dielectric beams because of their large size. Large radomes are typically shaped like a spherical dome, as shown in Fig.1

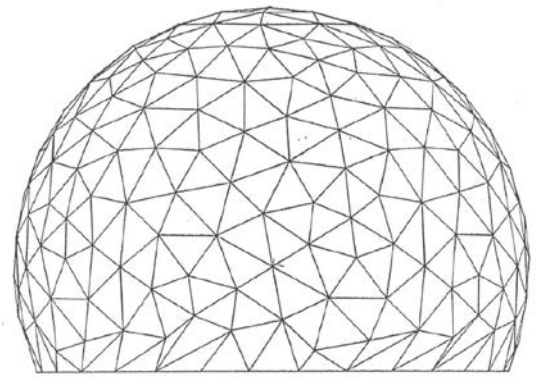

Fig.1-Geometry of a typical space frame radome.

This spherical shape for the radome is chosen not only because of structural and manufacturing considerations, but also because it provides the desired symmetry when the enclosed antenna performs scanning. From an electrical viewpoint, the beams and the window panels may be regarded as a collection of scatterers, which scatter the energy incident upon them from the transmitting antenna. In microwave applications, the window panels have little effect (especially for frequencies below X band) hence, the presence of the radome can be determined solely by evaluating the scattering properties of the beams and superimposing the effects in the far field. The radome is designed to have a quasi-random geometry to reduce the cumulative effect of scattering from the beams. The degree of randomness of the beam geometry can increase with a decrease in the beam length. However, such a decrease in the beam length also has associated negative effects, such as the increase in the total blockage due to the beams and decrease in the cost effectiveness of the panel manufacturing process. Consequently, there is a trade-off issue when randomness is considered in the design process of the radome. The frequency bandwidth of the radome, in terms of transmission losses and sidelobe perturbation performance, is determined by the combined effect of the panels and its beams. The panels are usually thin low-loss plastic membranes for metal and dielectric space frames, or A-sandwich type of panels for the sandwich radomes. The panels exhibit a wide frequency bandwidth, which normally does not limit the overall radome performance. The physical dimensions of the beams are determined by the stresses they have to withstand due to all environmental and physical loads, including extremely high wind-loading. Those beams may degrade the total system performance by introducing high levels of scattering which would limit the operational frequency bandwidth of the radome. The analysis of the scattering effect of space-frame radomes was first conducted by Kay [1].

Reduction of the scattering effect from the beams entails two steps:

(i) Minimizing the scattering level from the individual beams;

(ii) Optimizing the radome geometry.

Various methods to reduce the scattering effects from the beams, either as individuals or as an assembly in a space-frame radome are described in the paper and their effects on the radiation characteristics of an antenna enclosed in the radome are reviewed.

## II. SCATTERING FROM AN INDIVIDUAL BEAM

Scattering from metal and dielectric beams vary with frequency and is contributed by the electric polarization currents induced in the beams. This effect can be

characterized by the induced field ratio (IFR) [2] and the beam scattering pattern. The IFR parameter determines the scattering level from a beam of infinite length compared to the scattering from an aperture with the beam dimensions. The IFR of an ideal invisible beam is equal to zero and achieving this would be the design goal for a good space-frame radome. A metal beam which causes only optical blockage has an IFR equal to 1 at an angle of $180^0$. Fig. 2 presented in [2], [3] shows the dependence of the IFR for a perfect electric conductor (PEC) cylinder, while Fig. 3 also from [2], [3] shows the same dependence for a dielectric cylinder with $\varepsilon_r$=5 for parallel and perpendicular polarizations.

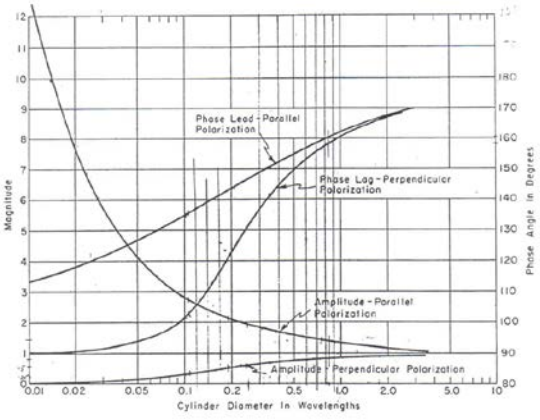


Fig.2-The IFR of a PEC cylinder as a function of its diameter in wavelengths [2], [3].

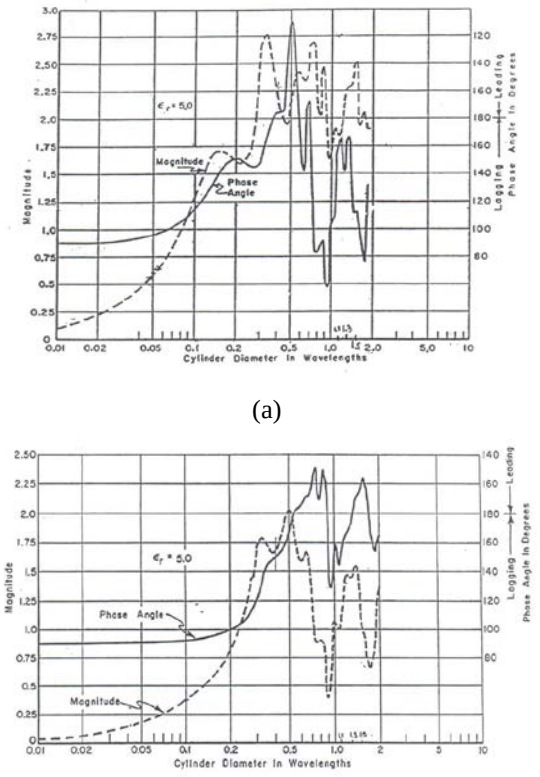


Fig.3- The IFR of a dielectric cylinder with $\varepsilon_r$=5 as a function of its diameter in wavelengths [2], [3] (a) parallel polarization, (b) perpendicular polarization.

As we can observe, the IFR for the metallic cylinder varies monotonically for both polarizations, and shows a decrease of the IFR amplitude with frequency for the parallel polarization. For high frequencies, the IFR tends to be 1 with an angle of $180^0$ (optical blockage) for both parallel and perpendicular polarizations. On the other hand, the picture is totally different for the dielectric cylinder. As one can observe, the IFR is very low for both polarizations at low frequencies, where the radius of the cylinder is small compared to the wavelength and therefore, the use of dielectric beams at low frequencies (less than 1 GHz) is attractive. However, as the frequency increases the induced polarization currents in the beam increase and, correspondingly, so does its IFR. Also, the IFR becomes oscillatory and the performance of the radome is not good over a broad frequency band. Similar results and trends are described in [4] and [5] for rectangular conductive and dielectric beams, respectively. Consequently, a dielectric space frame radome (DSF) is attractive for low frequencies (less than 1GHz), while a metal space frame (MSF) radome can operate above 1GHz over a wide frequency range. However, its minimal scattering losses are determined by the total optical blockage of the beams introduced in the antenna aperture. Another drawback of the scattering level for an MSF radome is an increase in the antenna sidelobe level above -25 dB for certain high- performance radar applications. Therefore, there is a real need to reduce the scattering level below the optical blockage for frequencies above 1 GHz.

Tuning techniques, such as insertion of conductive strips in the dielectric seams connecting the sandwich panels of the sandwich radome, are used [6], [7] to reduce the scattering level caused by the dielectric beams and design space-frame radomes to provide a performance better than that of MSF or DSF radomes. The currents induced in the conductive strips tend to offset the polarization currents induced in the seam and thereby reduce the tuned seam IFR. Fig. 4 shows the tuning mechanism with vertical and horizontal conductive strips.

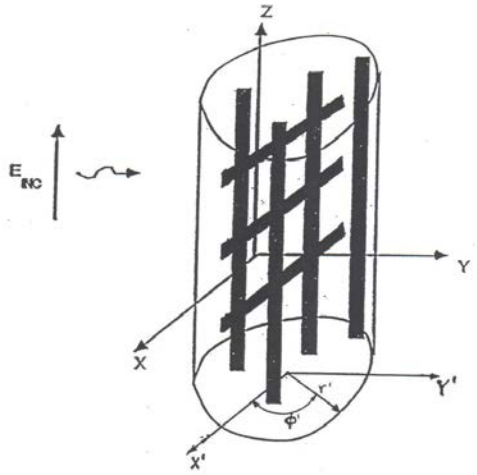


Fig.4- Basic geometry of a dielectric slab with tuning grid.

The problem of computing the scattering from a dielectric beam with a rectangular cross section loaded with conductive strips has been addressed by Michielssen and Mittra [8], [9] to solve its combined field integral equation using the Method of Moments (MoM).

Fig. 5 shows the IFR dependence of a typical tuned and untuned rectangular dielectric beam with dimensions 2" x 0.4". The electrical properties of the beam are $\varepsilon_r$=4.6 and tanδ=0.014. The beam is tuned with a grid of conductive strips located on its center line, spaced 0.277" apart and with a strip width of 0.062". The data presented is for the TM and normal incidence case. The computed and measured data are compared.

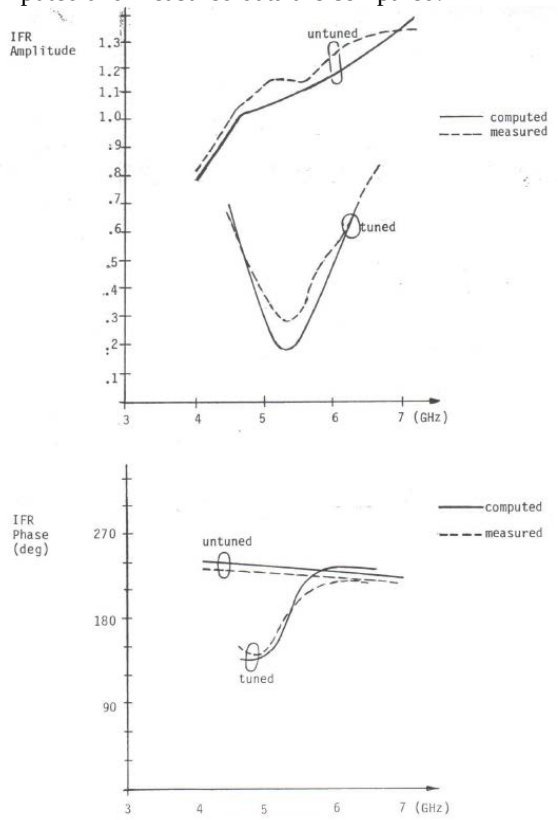


Fig.5- IFR as a function of frequency for a tuned/untuned dielectric beam 2" x 0.4" for vertical polarization at normal incidence.

At the tuning frequency of 5.6 GHz the magnitude of the IFR drops significantly in comparison to that of the untuned beam. In addition, the IFR phase goes through the $180^0$ value close to the tuning frequency, a feature common to resonant devices.

Fig.6 shows the field distribution (amplitude and phase) of the untuned and tuned beams inside the cross-section at 5.6 GHz.

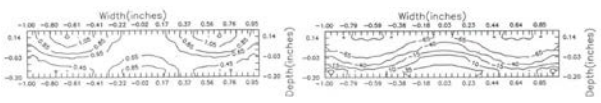

amplitude (dB) phase (deg.)

(a) untuned dielectric beam

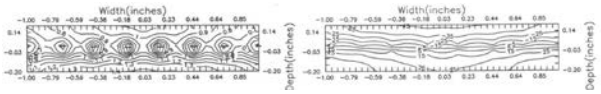

amplitude (dB) phase (deg.)

(b) tuned dielectric beam

Fig.6- Field distribution in an untuned and tuned dielectric beam at the tuning frequency (5.6 GHz) at normal incidence (a) untuned, (b) tuned.

As expected the total electric field goes to zero at the locations of the strips. Moreover, the phase of the electric field is relatively more uniform as compared to that of the untuned beam. The uniformity of the phase distribution is a good indicator of the transparency of the beam because it resembles the uniform phase front of the incident field. Fig.7 shows a comparison between the computed scattering pattern of the untuned and tuned dielectric beams at the tuning frequency of 5.6 GHz.

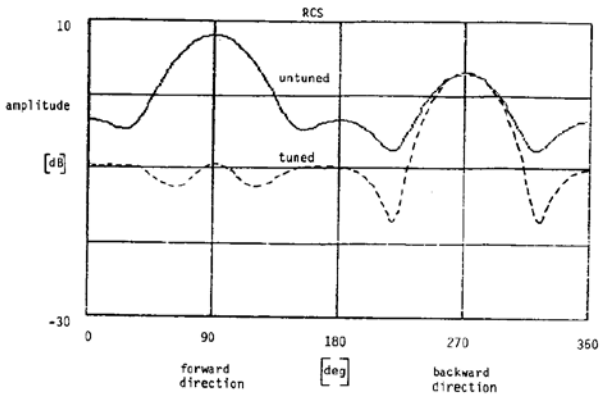


Fig.7- Scattering pattern for tuned and untuned beam at 5.6 GHz.

One can observe a significant reduction of the scattering levels in the forward direction as compared to that of the untuned beam.

The IFR's of two adjacent sandwich panels can be measured by the test set up shown in Fig. 8.

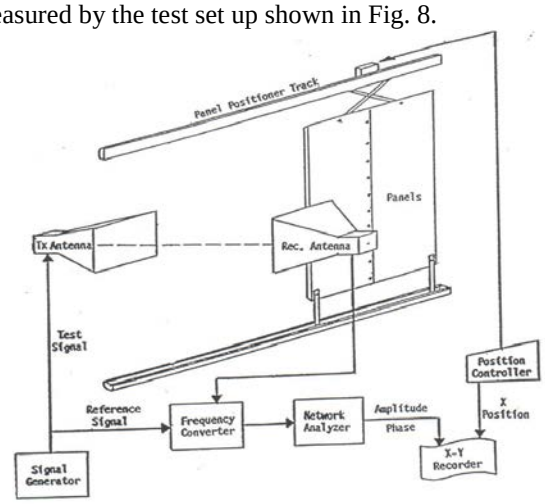


Fig.8-The measurement set-up for panel/seam test.

Two A-sandwich-type panels, with a seam in-between were moved on a track in front of a pair of receiving and transmitting horns. The amplitudes and phases variation

of the receiving signal were recorded throughout the panel movement. Using the measured phase and amplitude perturbation in the seam region, one can compute the IFR of the seam by using the formula given in [10]

$$IFR = \left(10^{0.05\Delta\alpha} e^{j\Delta\phi} - 1\right) \frac{e^{-j\pi/4}}{w} \sqrt{\frac{\lambda \eta_0 \eta_0'}{\eta_0 + \eta_0'}} \qquad (1)$$

where

$\Delta\alpha$ (dB) is the amplitude change due to the tested seam in the forward direction;

$\Delta\phi$ (deg.) is the phase change due to the tested seam in the forward direction;

$w$ is the width of the shadow area of the seam's geometrical cross-section on the incident wavefront.

$\lambda$ is the wavelength;

$\eta'_0$ is the distance between the tested seam and the transmitting horn;

$\eta_0$ is the distance between the tested seam and the receiving horn.

Typical recordings of signals (amplitude and phase) for both the parallel (TM case) and perpendicular (TE case) polarizations are shown in Fig.9.

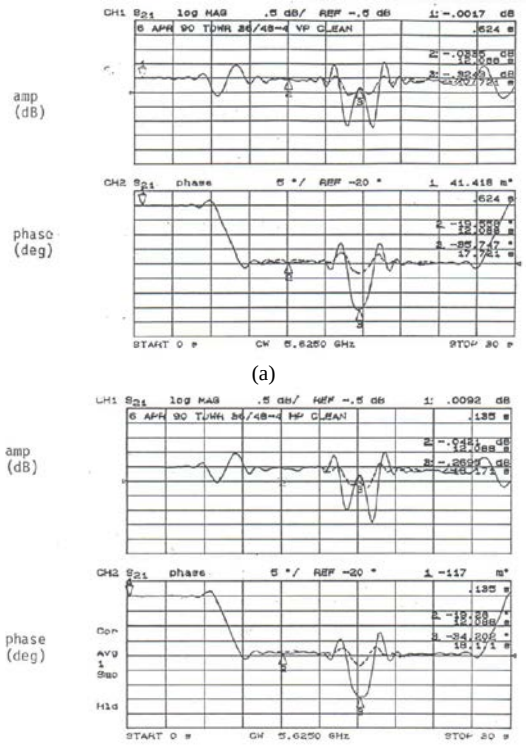


(a)

(b)

Fig. 9- Measured TL and IPD for tuned (----) and untuned (_____) beam. (a) vertical polarization, (b) horizontal polarization.

One can observe the reference signal before the panels cross the boresight line between the transmitting and receiving horns; the diffraction effect when the panels begin to cross this line; the insertion phase delay (IPD) and the transmission loss (TL) of the panel; and the phase and amplitude perturbations in the area of the seams. The recorded signal is symmetric with respect to the seam axis. The perturbation of the amplitude and phase in the seam region is significantly reduced for the tuned case. Moreover, one can observe a significant reduction in the IPD introduced by the seam for the tuned case.

## III. SCATTERING ANALYSIS OF THE BEAMS

The approach introduced by Kay in [1] is followed in this work to derive the expression for the perturbed far-field radiation pattern of the antenna enclosed by the radome. Applications of Kay [1] approach to MSF and DSF can be found in [11], [12], and to tuned and untuned sandwich radomes in [13]-[15]. Fig. 10 shows a schematic diagram of the scattering mechanism of the beams. The aperture of the antenna is chosen to be elliptical with its major axes $2a$ x $2b$ and its center is assumed to be offset from the radome center $(0, y_0, z_0)$. The coordinate system for the scattering analysis is shown in Fig. 10.

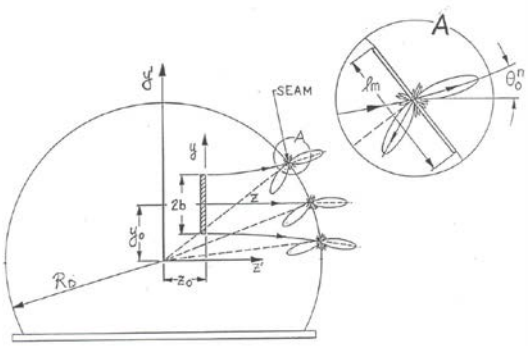


Fig.10-The geometry of the radome and the scattering mechanism.

Let the coordinates of the center of the $m^{th}$ beam be $(x_m, y_m, z_m)$ and let this beam be projected on the effective illuminated antenna aperture. The angle of inclination of the projected beam on the antenna aperture with respect to the $y$-axis is $\delta_m$. The peak of the scattering pattern from the $m^{th}$ beam is determined by the incident angle $(\theta_0^m, \phi_0^m)$ of the corresponding constituent ray of the Gaussian beam at its center, as shown in Fig.10. In this derivation we use the coordinate system $(\theta,\phi)$ where $\theta$ is the elevation angle measured in the $y$-$z$ plane and $\phi$ is the azimuthal angle measured from the $z$-axis in the $x$-$z$ plane. To determine the effect of perturbation due to the beam scattering, we initially compute the unperturbed far-field pattern of the antenna enclosed by the radome, and then superpose this result to the scattering pattern of the beam assembly.

In the scattering analysis we make the following assumptions that are valid approximations for the purpose of computing the perturbed far-field radiation pattern:

(i) The field incident upon the radome due to the enclosed antenna can be represented by using a divergent Gaussian beam model. Further, only the beams within the incident beam of the enclosed antenna contribute to the scattering.

(ii) The total scattered field from the beams is assumed to be a superposition of all individual beams. Mutual coupling and multiple scattering effects are negligible.

(iii) The field incident upon a particular radome beam member does not vary significantly over the extent of the member.
(iv) The field radiated by the $m^{th}$ beam is equivalent to that arising from a straight rectangular current strip projected on the antenna aperture with length $l_m$, width $w_m$ and with constant transverse and axial current distributions.

To determine the perturbation due to the beam scattering, we initially compute the unperturbed far-field pattern of the antenna enclosed in the radome. In our analysis, we have assumed that the aperture distribution $f(x,y)$ [14] of the elliptical aperture of the antenna with dimensions $2a \times 2b$, is expressed as

$$f(x,y) = C + (1-C)\left[1 - \frac{x^2}{a^2} - \frac{y^2}{b^2}\right]^p \tag{2}$$

where $C$ is the pedestal illumination and $p$ is an exponential factor, which determines the shape of the aperture distribution. Given the aperture distribution $f(x,y)$, one can compute the far field pattern $F(\theta,\phi)$ [16], which can be expressed in a closed form as,

$$F(\theta,\phi) = \pi a^2 \cos\alpha \left[ C\frac{2J_1(u)}{u} + (1-C)\frac{2^{p+1}\Gamma(p+1)J_{p+1}(u)}{u^{p+1}} \right] \tag{3}$$

where $\cos\alpha = b/a$, $J_p(u)$ is the Bessel function of $p^{th}$ order, $\Gamma(p+1)$ is the Gamma function and $u = ka\sin\theta\left(1 - \sin^2\phi\sin^2\alpha\right)^{1/2}$. To evaluate the field incident upon the beams, the radiated near field from the elliptical aperture can be approximated by a Gaussian beam [17] with two independent waists $W_{el}(z)$ and $W_{az}(z)$ in elevation and azimuth, respectively. The waist $W(z)$ is given by [17],

$$W(z) = W_0\left[1 + \left(\lambda z / \pi W_0^2\right)^2\right]^{1/2} \tag{4}$$

where, $W_0$ is the waist of the Gaussian beam at $z$=0 and it can either be $W_{0,el}$ (elevation) or $W_{0,az}$ (azimuth). $W_0$ can be computed by equating the actual 3dB beamwidth of the aperture to the 3dB beamwidth of the Gaussian beam approximation. The radius of curvature $R(z)$ of the Gaussian beam is given by [17],

$$R(z) = z\left[1 + \left(\pi W_0^2 / \lambda z\right)^2\right]. \tag{5}$$

There are two radii of curvature, $R_{az}$ and $R_{el}$ in azimuth and elevation, respectively. Given $W(z)$ and $R(z)$, one can compute the field intensity $f(x,y,z)$ of the Gaussian beam at any distance $z$ from the antenna aperture, by using:

$$f(x,y,z) = \left[\frac{W_{0,el}W_{0,az}}{W_{el}W_{az}}\right]^{1/2} e^{-\frac{x^2}{W_{az}^2}-\frac{y^2}{W_{el}^2}} e^{-jkz} e^{-j\frac{\pi}{\lambda}\left(\frac{x^2}{R_{az}}+\frac{y^2}{R_{el}}\right)} e^{j\tan^{-1}\left(\frac{\lambda z}{\pi W_{0,el}W_{0,az}}\right)}. \tag{6}$$

One can observe that the intensity of the electric field decays exponentially transverse to the propagation $z$-axis. Moreover, the intensity of the Gaussian beam drops by more than 30 dB at a lateral distance of $4W_{az}$ in $x$ direction and $4W_{el}$ in $y$ direction. Given this, the scattering effects from beams beyond a lateral distance of $4W_{az}$ ($x$ direction) and $4W_{el}$ ($y$ direction) can be ignored.

Using the approximations mentioned above, the far-field scattering pattern $I_m(\theta,\phi)$ from the $m^{th}$ beam can be written as,

$$I_m(\theta,\phi) = w_m l_m \frac{\sin A_m}{A_m}\frac{\sin B_m}{B_m} e^{jk(x_m u_m + y_m v_m + z_m d_m)} \tag{7}$$

where,

$$\begin{aligned} u_m &= \cos\left(\theta - \theta_0^m\right)\sin\left(\phi - \phi_0^m\right) \\ v_m &= \sin\left(\theta - \theta_0^m\right) \\ d_m &= \cos\left(\theta - \theta_0^m\right)\cos\left(\phi - \phi_0^m\right) \end{aligned} \tag{8}$$

$$\begin{aligned} A_m &= \frac{kW_m}{2}\sin\theta'\cos\left(\phi' + \delta_m\right) \\ B_m &= \frac{kl_m}{2}\sin\theta'\sin\left(\phi' + \delta_m\right) \\ \sin\theta' &= \left[\sin^2\left(\theta - \theta_0^m\right) + \cos^2\left(\theta - \theta_0^m\right)\sin^2\left(\phi - \phi_0^m\right)\right]^{1/2} \\ \sin\phi' &= \frac{\sin\left(\theta - \theta_0^m\right)}{\sin\theta'} \end{aligned} \tag{9}$$

The scattering from the beams is weighted by the antenna illumination function $f(x_m,y_m,z_m)$, given by (6) which is proportional to the IFR, and the scattering pattern $I_m(\theta,\phi)$ given by (7). Thus the total scattered field from $M$ beams can be written,

$$F_s(\theta,\phi) = \sum_{m=1}^{M} g_m I_m\left(\theta,\phi/\theta_0^m,\phi_0^m\right) f_m\left(x_m,y_m,z_m\right) \tag{10}$$

where [12]

$$g_m = g_{\parallel}\cos^2\delta_m + g_{\perp}\sin^2\delta_m. \tag{11}$$

and $g_{\parallel}$, $g_{\perp}$ are the parallel and perpendicular components of the beam IFR. By combining the unperturbed pattern of the antenna $F(\theta,\phi)$ given by (3) and the scattered pattern from the beams $F_s(\theta,\phi)$ given by (10), one can compute the perturbed pattern $F'(\theta,\phi)$ by expressing it as

$$F'(\theta,\phi) = F(\theta,\phi) + F_s(\theta,\phi) \tag{12}$$

As an example of the scattering effect of the beams, we consider a vertically polarized antenna aperture 27' x 2' operating at 1.09GHz, which is enclosed in a 56 foot tuned sandwich radome. We assume that the aperture taper is 15 dB, i.e., $p$=2. The measured parallel polarization IFR is -0.013+j0.013 and the perpendicular polarization IFR is -0.12+j0.001, for a seam width of 4 inches. The Gaussian beam spreading results in an illuminated aperture on the radome surface of 29.6' x 13.2', which indicates that more seams are illuminated than is evident from the projected 27' x 2' aperture. Figure 11 shows the comparison between the computed scattering patterns with and without the inclusion of the divergence effect of the radiating aperture.

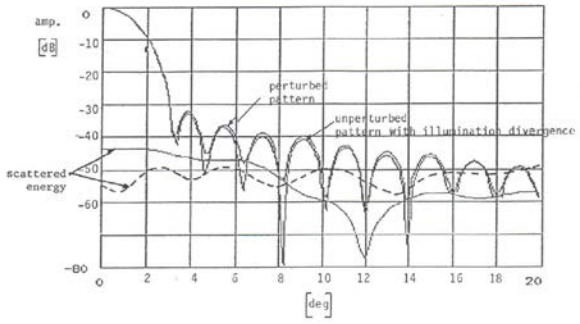


Fig.11-Computed azimuth radiation patterns (perturbed and unperturbed) and the scattering pattern due to the beams with (dashed) and without (solid) the divergence effect @ 1.09 GHz.

One can observe that the divergence causes the scattered energy from the seams to be more uniformly distributed over a wider sector. The total transmission loss (with illumination divergence) from the radome improves from 0.06 dB to 0.02 dB, and the scattering level becomes more uniform.

*A. Radiation parameters affected by the scattered energy from the beams.*

The scattered energy by the beams affects a number of radiation parameters [18], as for example:

(i) Transmission loss.
(ii) Sidelobe level increment of the enclosed antenna
(iii) Null depth in a difference pattern
(iv) Beamwidth change
(v) Boresight error
(vi) Boresight error slope
(vii) Cross-polarization ratio
(viii) Antenna noise temperature

*(a)Transmission Loss*

The transmission through the radome not only depends upon the construction of the radome window, but also upon the antenna look angle, the field distribution over the antenna aperture, the location of the antenna inside the radome and the radome/antenna size ratio. Using ray tracing methods [1] the transmission through the radome can be determined by summing up the losses from all rays, which have different weight functions and look angles. The total loss through the radome, $L_t$ is given by

$$L_t = L_w + L_j \quad ,$$

where,

$L_w$- transmission loss due to the radome wall in dB

$L_j$- transmission loss due to the beams scattering in dB

$$L_j = 10 \cdot \log\left|1 + \rho_s \cdot \mathrm{Re}\{IFR\}\right|^2 \qquad (13)$$

$\rho_s$- physical blockage of projected beams on the antenna aperture.

*(b) Sidelobe level increment*

At each angle, the energy scattered by the radome and computed by the model presented in [1] interferes with the radiated energy according to the amplitude and phase relationship between these two contributions. A sidelobe level (*SL)* in (dB) below the peak of the sum pattern is affected by the scattered energy (*SE)* in (dB) relative to the peak. The resulting sidelobe perturbation $\Delta SL$(dB) can be approximated by

$$\Delta SL = 20\log\left(1+10^{(SE-SL)/20}\right) \qquad (14)$$

*(c) Null depth increment*

The scattered energy, whether it is co-polarized or cross-polarized, fills in the null of a monopulse system. The on-axis contribution of the scattered energy interacts with the weak energy in the null pattern radiated in this direction and affects the pattern according to the amplitude and phase relationship between the two sources. The null's depth increment in the worst case can be approximated by eq. (14), in which *SL*(dB) can be replaced by the null depth.

*(d) Beamwidth change*

The interference of the scattered energy with the main beam energy causes a $\Delta\theta$ change in the antenna beamwidth *BW*. Maximum effect occurs when both sides of the beam are affected in the same way, either with in-phase or out-of-phase combination. The approximated antenna beamwidth variation at the 3dB points is described in [18] and is given by

$$\Delta\theta = \frac{2 \cdot BW \cdot 20\log\left(1+10^{\frac{SE+3}{20}}\right)}{12} \quad . \qquad (15)$$

This formula assumes a phase addition of the antenna field and the radome scattering field at the -3dB points.

*(e) Boresight error*

Boresight error (*BSE*) results from an imbalance between the two halves of the antenna. The source of the asymmetry may be a result of the difference in panel construction or the presence of more beams in front of one side of the antenna. The contribution of the beams is a function of their distribution in front of the antenna. An approximate formula [18], which estimates the beam induced boresight error reads:

$$BSE(rad) = \frac{0.27 \cdot \lambda \cdot L \cdot W \cdot \left|\mathrm{Im}(IFR)\right|}{R^3} \qquad (16)$$

where,

*W*-the width of the beam

*L*- the average length of the beams

*R*- the radius of the antenna

$\lambda$- the wavelength

This formula assumes that there is an entire beam on one side of the aperture, uncompensated by the presence of another beam on the opposite half. The actual imbalance is smaller in the large-antenna case.

*(f) Boresight-error slope*

The rate of change of the boresight error is dependent on the change in the amount of beams in front of the antenna. Following [18] it can be approximated by

$$Slope = BSE / \theta_r \quad (17)$$

where,
BSE- boresight error
$\theta_r$- subtended angle of the radome's beam from the antenna center

*(g) Cross-polarization ratio*

The way in which the radome affects cross-polarization is also the same way it affects the sidelobes; that is, the scattered energy vectorially adds to the field radiated by the antenna without the radome. The principal difference here is that the energy scattered into the cross-polarization field must be less than half of the co-polarized scattered energy; thus the scattered-energy level used for the effect on cross-polarization energy is 3 dB lower for the change in the sidelobe level calculation.

*(h) Antenna noise temperature*

The noise temperature contribution due to the radome includes three factors:
(i) Noise temperature contribution, $NT_1$ due to absorption in the radome window
(ii) Noise temperature contribution, $NT_2$ due to reflection from the radome window
(iii) Noise temperature contribution, $NT_3$ due to scattering from the beams

The noise contribution due to absorption in the radome window can be approximated by $NT_1=300*P_a$, where $P_a$ is the amount of energy absorbed in the radome windows. When computing the reflection contribution, it is assumed that half of this energy is reflected to the cold atmosphere and half to the warm earth (300°K), therefore $NT_2=150*P_r$, where $P_r$ is the amount of energy reflected by the radome windows. In the scattering case, the noise temperature contribution is dependent on the antenna elevation angle. Thus, for a typical 10° elevation angle, we assume that half of the scattered energy goes forward to the cold atmosphere and the other half backward; furthermore half of the backward energy is reflected by the antenna reflector back to the cold atmosphere. Under this assumption we obtain, $NT_3=75*P_s$, where $P_s$ is the amount of energy scattered by the radome beams.

## IV. GEOMETRY OPTIMIZATION

The total scattering effect of the antenna from all the beams in front of the aperture is computed by superposing all of the scattering effects from the individual beams. Optimization of the radome geometry takes into consideration factors such as minimization of the total seam length, increase in panel dimensions, minimization of the total number of parallel beams and uniform beam density throughout the antenna/radome scan angles. Fig.12 shows the difference in the beams scattering level and its distribution for a radome geometry projected on a circular antenna aperture for the case of a parallel (bad) geometry, and its comparison with the distribution for the quasi-random (good) geometry.

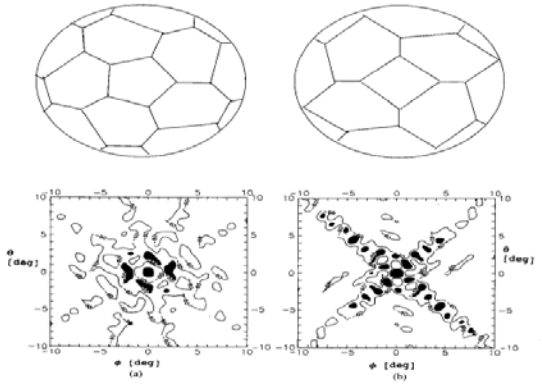


Fig. 12- Comparison of the radome scattering patterns between (a) quasi-random and (b) parallel geometries.

One can observe that the scattered field for the case of the quasi-random geometry is more uniformly distributed, and has a lower intensity in comparison to that of the parallel geometry. Accordingly, the effect on the radiation characteristics of the antenna enclosed by the radome with quasi-random panelization is lower. Fig.13 shows the difference in the seams scattering level, and distributions for a quasi-random radome geometry with and without tuned seams.

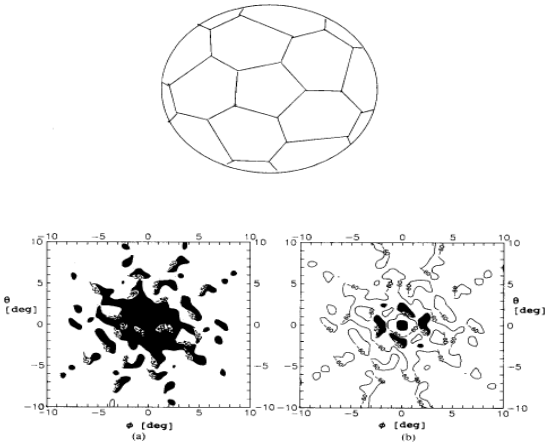


Fig.13- Comparison between the scattering patterns of a quasi-randomized geometry with (a) untuned and (b) tuned seams.

The results in Fig.13 demonstrate the significance of tuning the seams in a sandwich radome. Another important factor in the radiation characteristics of an enclosed antenna in a sandwich radome is the variability of the blockage by the seams, through the radome with the antenna aspect angle. In a well-designed radome, the blockage to the antenna is almost independent of the aspect angle of the antenna relative to the radome, while large variability may be encountered in a badly designed radome. Fig.14 shows the variability of the seams blockage due to seams in a "good" and a "bad" sandwich radome design.

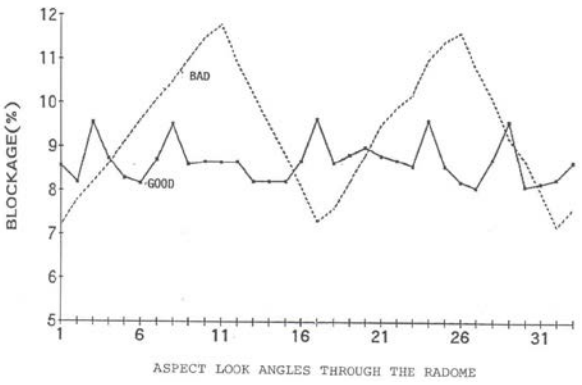


Fig.14- Beams blockage dependence on aspect angle for a "bad" and a "good" (uniform density) radome geometry.

## VI. CONCLUSIONS

Scattering effects from the beams play an important role in the design of large ground-based radomes. To obtain a high-performance radome, one should consider reducing both the scattering from the individual beams and optimizing the beam geometry.

The scattering from the beams affect many radiation characteristics of the antenna and not just the transmission loss. In this paper, we have reviewed the analytical and numerical tools to analyze these effects. The analysis shows that the DSF radome performs well for low frequencies, while the MSF radome has a wide frequency range, although its performance is limited. Finally, if we require a high-performance radome operating in a limited frequency range we should consider the use of a tuned sandwich radome.

## REFERENCES

[1] A.F. Kay, "Electrical design of metal space frame radomes," *IEEE Trans. Antennas Propag.*, vol. AP-13, pp.188-202, March 1965.

[2] P.D. Kennedy,"An analysis of the electrical characteristics of structurally supported radomes", Report by Ohio State University under contract AF-30 (602)-1620, Nov.15, 1958.

[3] J.A. Vitale," Large radomes", Microwaves Scanning Antennas, ed. by R.C. Hansen, Ch. 5, Academic Press 1966.

[4] M.G. Andreasen,"Scattering by conducting rectangular cylinders", *IEEE Trans. Antennas Propag.*, vol. AP-12, pp.746-754, Nov. 1964.

[5] J.H. Richmond,"Scattering by a dielectric cylinder of arbitrary cross-section shape", *IEEE Trans. Antennas and Propag.*, pp.334-341, May 1965.

[6] K.C. Chang and A.P. Smolski, "The effect of impedance matched radomes on SSR antenna systems," *IEEE Conf. Proc. Radar 87*, London, U.K., Oct. 1987, pp.155-159.

[7] F.C. Smith, B. Chambers and J.C. Bennett, "Improvement in the electrical performance of dielectric space frame radomes by wire loading", *IEEE Symp. on Antennas and Propag.*, ICAP 89, pp.530-534, Coventry, UK, April 1989.

[8] E. Michielssen and R. Mittra,"RCS reduction of dielectric cylinders using a simulated annealing approach", *IEEE Symp. on Antennas and Propag.*, Dallas, Tx, May 1990, pp.1268-1271.

[9] E. Michielssen and R. Mittra,"TE plane wave scattering by a dielectric cylinder loaded with perfectly conducting strips", *IEEE Symp. on Antennas and Propag.*, Dallas, Tx, May 1990, pp.125.

[10] W.V.T. Rusch, J.A. Hansen, C.A. Klein, and R. Mittra, "Forward scattering from square cylinders in the resonance region with application to aperture blockage,"*IEEE Trans. Antennas Propag.*, vol. AP-24, pp. 182-189, March 1976.

[11] S.R. Katashaya and B.G. Evans,"Depolarization properties of metal space frame radomes for use in satellite communication systems", *Int'l Journal of Satellite Communications*, vol.2, 1984, pp. 61-72.

[12] K.C. Chang and A.P. Smolski,"A radome for air traffic control SSR radar systems", *IEEE Conf. Proc. Radar 87*, London, U.K., Oct. 1987, pp.160-164.

[13] R. Shavit, A.P. Smolski, E. Michielssen, and R. Mittra, "Scattering analysis of high performance large sandwich radomes", *IEEE Trans. Antennas and Propag.*, Vol. 40, pp. 126-133, February 1992.

[14] G. Virone, R. Tascone, G. Addamo and O.A. Peverini,"A design strategy for large dielectric radome compensated joints", *IEEE Antennas and Wireless Propag. Letters*, Vol. 8, pp. 546-549, 2009.

[15] S. Mishra, M. Sarkar and A. Daniel,"Optimization of radome wall and joint for X-band reflector antenna using Floquet modal analysis", *Journal of Electromagnetic Waves and Applications*, Vol.28, pp.1257-1268, July 2014.

[16] S. Cornbleet,"Microwave optics", Academic Press Inc., London, 1976.

[17] P.F. Goldsmith," Quasi-optical techniques at millimeter and submillimeter wavelengths", Infrared and Millimeter Waves, vol.6, ed. by K.J Button, Ch. 5 (New York Academic 1982).

[18] M. Skolnik, "Radar Handbook, "(2nd edition), Wiley, 1990.

**List of Acronyms**

IFR-induced field ratio

PEC-perfect electric conductor

DSF-dielectric space-frame

MSF-metal space-frame

MoM-method of moments

TL-transmission loss

IPD-insertion phase delay

SL-sidelobe level

SE-scattered energy

BSE-boresight error